BIOCHEMISTRY
including biophysical chemistry & molecular biology

Article

pubs.acs.org/biochemistry

Modifying Caspase-3 Activity by Altering Allosteric Networks

Christine Cade,[†] Paul Swartz,[†] Sarah H. MacKenzie,[†] and A. Clay Clark*[,†,‡]

[†]Department of Molecular and Structural Biochemistry and [‡]Center for Comparative Medicine and Translational Research, North Carolina State University, Raleigh, North Carolina 27695, United States

Supporting Information

ABSTRACT: Caspases have several allosteric sites that bind small molecules or peptides. Allosteric regulators are known to affect caspase enzyme activity, in general, by facilitating large conformational changes that convert the active enzyme to a zymogen-like form in which the substrate-binding pocket is disordered. Mutations in presumed allosteric networks also decrease activity, although large structural changes are not observed. Mutation of the central V266 to histidine in the dimer interface of caspase-3 inactivates the enzyme by introducing steric clashes that may ultimately affect positioning of a helix on the protein surface. The helix is thought to connect several residues in the active site to the allosteric dimer interface. In contrast to the effects of small molecule allosteric regulators, the substrate-binding pocket is intact in the mutant, yet the enzyme is inactive. We have examined the putative allosteric network, in particular the role of helix 3, by mutating several residues in the network. We relieved steric clashes in the context of caspase-3(V266H), and we show that activity is restored, particularly when the restorative mutation is close to H266. We also mimicked the V266H mutant by introducing steric clashes elsewhere in the allosteric network, generating several mutants with reduced activity. Overall, the data show that the caspase-3 native ensemble includes the canonical active state as well as an inactive conformation characterized by an intact substrate-binding pocket, but with an altered helix 3. The enzyme activity reflects the relative population of each species in the native ensemble.

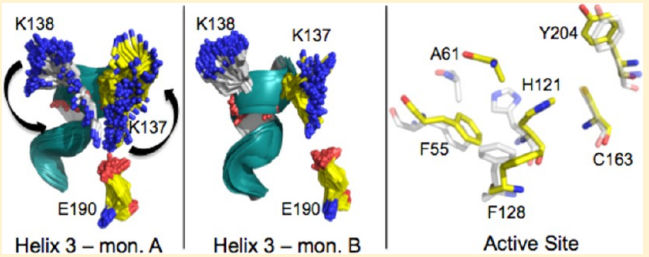

Caspases have a number of conformational states in the zymogen as well as the cleaved forms (Figure 1). The procaspase monomer assembles to an inactive dimer either through folding and assembly, in association with death receptors in the cell, or in the presence of kosmotropes *in vitro*.[1−4] Depending on the procaspase, the dimer also forms an active yet uncleaved conformation.[5] In general, caspases are activated by cleavage of the polypeptide chain in a region that separates the large and small subunits (intersubunit linker) (see ref 2 for a review of caspase structures and activation). The cleaved caspase is found in an inactive zymogen-like form, where the active sites are not well ordered, as well as a mature, active conformation with intact active sites. The equilibrium between the apo-caspase (inactive) and the mature caspase is modulated by binding of substrate in the active site or by binding of inhibitors in allosteric sites.[6]

All caspases recognize aspartate in the P1 position of the substrate, so the design of activity-based inhibitors with specificity for individual caspases has been particularly challenging. Inhibitors with selectivity to the various caspases are of interest because of the differential role of caspases in the development of certain tissues,[7,8] the involvement of caspases in neurodegeneration,[9,10] and dysregulation of caspases in cancers.[11,12] In contrast to the conserved active site, the dimer interface is less conserved among the caspase family members and has been shown to be an allosteric site.[6] Allosteric small molecules that bind at the dimer interface of several caspases, including caspase-3, induce large conformational changes in active site loops, resulting in a zymogen-like conformation that is inactive (see Figure 1).[6,13] Notably, the substrate-binding loop, called L3 (Figure 2), is extended toward solvent rather than forming a groove on the protein surface as observed in the active enzyme. Overall, the data from small molecule allosteric inhibitors suggest that caspase allostery involves large conformational changes between the canonical active state, with intact active site loops competent to bind substrate, and a zymogen-like form with unordered active site loops unable to bind substrate (Figure 1).

In contrast to the two-state allosteric model, we have shown that the mutation of V266 to histidine in the dimer interface, near the binding sites for allosteric inhibitors, produces very subtle conformational changes that nonetheless completely inactivate the enzyme. In the procaspase, the mutation decreases the rate of dimer assembly,[14] resulting in a hysteresis, although the protein is fully dimeric at equilibrium. In the mature caspase, steric clashes with the bulkier H266 on β-strand 8 disrupt a conserved network of water molecules and shift the neighboring Y195 (β-strand 7) toward T140 in helix 3 (Figure 2).[15,16] In wild-type caspase-3, Y195 hydrogen bonds with T140 and with E190 through two water molecules (Figure

Received: July 16, 2014
Revised: October 10, 2014
Published: October 24, 2014

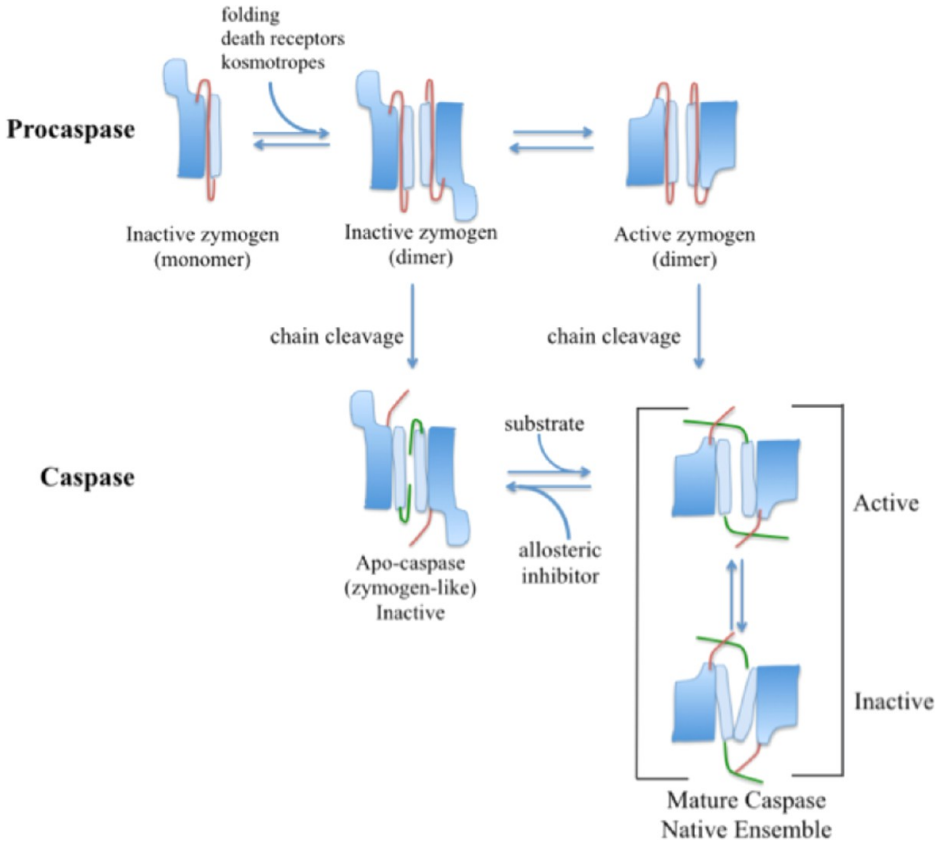

Figure 1. Conformational states of caspases. The procaspase monomer forms dimers either through folding and assembly, where the dimer is the most stable form (effector caspases, for example), through interaction with death receptors (initiator caspases, for example), or through the action of kosmotropes (sodium citrate, for example). The dimer of the zymogen contains inactive and active conformations. Cleavage of the intersubunit linker (red loop) results in the formation of two active site loops, called L2 and L2′ (see Figure 2), colored green and red, respectively, and separation of the two subunits (large subunit, dark blue; small subunit, light blue) to form the protomer. In the inactive zymogen-like caspase form, loop L2′ (green) remains bound in the dimer interface and the active site loops are disordered. In the active caspase, L2′ interacts with L2 of the opposite protomer and stabilizes the active conformation. The equilibrium between the active and zymogen-like caspase is affected by binding of substrate in the active site or allosteric inhibitor to the dimer interface (or other allosteric sites). As described here, the mature caspase ensemble also contains an inactive conformer characterized by an intact substrate-binding pocket and destabilized helix 3.

2b, red spheres). In the V266H variant, the shift in Y195 results in a direct hydrogen bond with T140. A new water molecule replaces the hydroxyl group (compared to its position in the wild-type enzyme) to maintain the hydrogen bonding network with E190 (Figure 2b, yellow sphere). In addition, a salt bridge between K137 (helix 3) and E190 is disrupted in the V266H variant (Figure 2b). The presence of H266 results in movements of two surface β-strands [strands 4 and 5 (Figure 2a)] such that F128 (β-strand 4) clashes with M61, which in turn clashes with the catalytic residue H121 (Figure 2c). The movement of H121 disrupts hydrogen bonding with active site loop 1 (called L1), which is mostly disordered in the crystal structure. Molecular dynamics simulations of caspase-3-(V266H) revealed that the N-terminus of helix 3 transiently rotates into the dimer interface, causing a distortion of the substrate-binding pocket.[16] These subtle changes led us to suggest that one should consider caspase-3 conformational dynamics as containing active and inactive ensembles rather than a single active conformation and a single inactive conformation as in the two-state allosteric model (Figure 1, mature caspase native ensemble).[16]

On the basis of our previous mutational and structural studies of the interface allosteric site,[15−19] we examined the putative allosteric network to gain insight into the inactive ensemble of caspase-3. Here, we describe two main groups of mutations in the allosteric network. First, we generated a set of single mutants to introduce steric clashes that mimic the V266 to histidine mutation at regions away from the allosteric interface (Table 1, "steric clash" mutants; Figure 2b,c). Second, we generated a set of double mutants in the context of V266H designed to relieve steric clashes induced by H266. These mutants are predicted to restore activity in the H266 variant (Table 1, "restorative" mutants; Figure 2b). We also examined the importance of a salt bridge in helix 3 that is close to the dimer interface but is absent in the V266H mutant. In this case, we replaced K137 and E190 with alanine (Table 1, "salt bridge" mutants; Figure 2b). Finally, we examined the mutation of T140 to valine to probe the importance of hydrogen bonding on stabilizing helix 3 (Table 1, "hydrogen bonding" mutants; Figure 2b).

We show that relieving steric clashes in the allosteric network introduced by the V266 to histidine mutation results in increased activity. We also show that the "steric clash" mutants effectively mimic V266H. Surprisingly, however, helix 3 was able to accommodate phenylalanine at position 140 and gained a new mechanism to stabilize the helix. Overall, the data from enzyme activity assays, molecular dynamics simulations, and X-ray crystallography show that the native ensemble of mature

dx.doi.org/10.1021/bi500874k | *Biochemistry* 2014, 53, 7582−7595

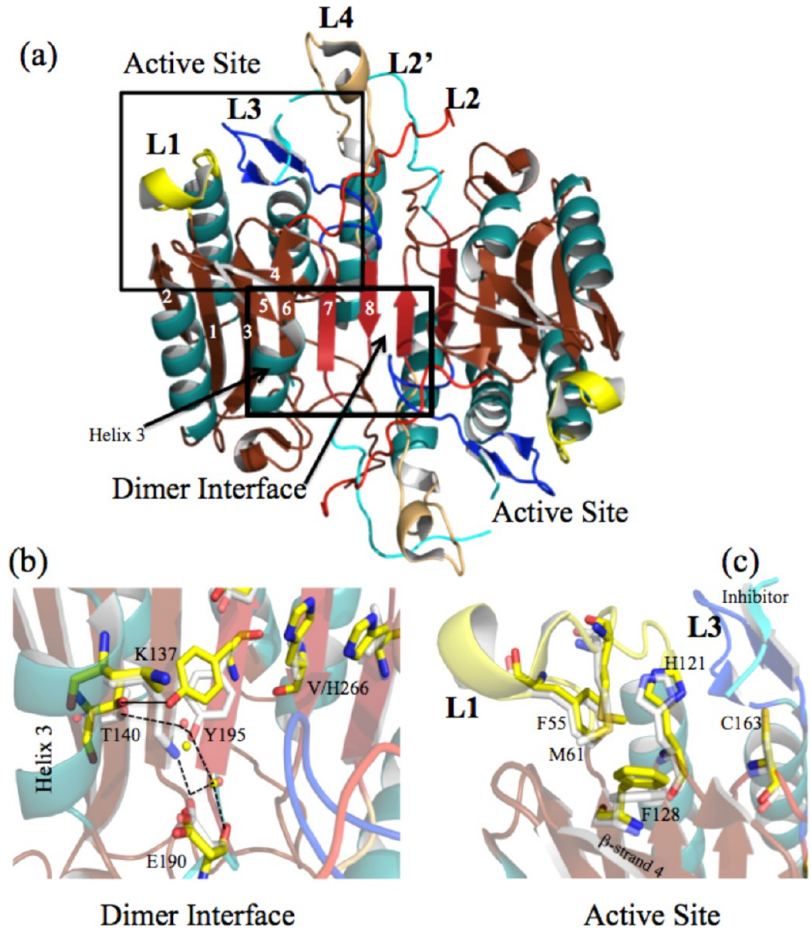

Figure 2. Comparison of wild-type and V266H caspase-3 structures. (a) Caspase-3 structure (PDB entry 2J30) highlighting β-strands 1−8 and active site loops L1−L4 and L2′ in one protomer. The two boxes indicate regions of mutations in the dimer interface and active sites. (b) H266 causes Y195 to move toward T140 (helix 3) (PDB entry 4EHA). A salt bridge between K137 and E190 is also disrupted. Red spheres indicate water molecules in WT caspase-3, and yellow spheres indicate water molecules in caspase-3(V266H). The dashed lines indicate hydrogen bonds in wild-type caspase-3, and the solid line indicates a hydrogen bond in caspase-3(V266H). (c) Comparison of active site residues F128, M61, F55, H121, and C163 for WT and V266H proteins. For panels b and c, amino acids are colored yellow for the V266H variant and gray for WT caspase-3.

Table 1. Allosteric Mutants Sorted by Category and Location

	steric clash	restorative	control	hydrogen bonding or salt bridge
dimer interface	T140F	T140G/V266H	T140M	
	T140G	Y195A/V266H	Y195A	
		Y195F/V266H	Y195F	
active site	F55W	M61A/V266H	M61A	
	F55Y	F128A/V266H	F128A	
helix 3				T140V
salt bridge				K137A
				E190A

caspase-3 contains a conformation with a mostly intact substrate-binding pocket but with a destabilized helix 3, which appears to lower activity by distorting two surface β-strands near the active site.

MATERIALS AND METHODS

Cloning, Expression, and Purification. Site-directed mutagenesis was performed as described previously with plasmids pHC332 (WT caspase-3),[20] pHC33203 [caspase-3(V266H)],[15] and pHC332125 [caspase-3(Y195A)] and the primers listed in Table S1 of the Supporting Information. *Escherichia coli* BL21(DE3)pLysS cells were transformed with each of the plasmids, and proteins were expressed and purified as previously described.[15−17,21,22]

Crystallization and Data Collection. With the exception of the T140G variant, caspase-3 variants were crystallized in the presence of Ac-DEVD-CMK as previously described.[16,17] In the case of T140G, the protein was crystallized in the presence of Ac-DEVD-CHO. Most crystals appeared within ∼3 days, although some took as long as 3 weeks to grow. Cryoprotectants included 20% PEG 400/80% reservoir solution, 20% glycerol/80% reservoir solution, 20% MPD/80% reservoir solution (most successful), or 10% MPD/90% reservoir solution systems. Data sets were collected, and structures were determined by molecular replacement using the wild-type caspase-3 structure for initial phasing (PDB entry 2J30); structural models were refined using Phenix, as previously described.[16] Of the 17 proteins listed in Table 2, we report the structures of all proteins except for the T140M and F55Y variants. The 15 structures determined were within a 0.3 Å rmsd of wild-type caspase-3 (Table S2 of the Supporting Information). A summary of the data collection and refinement statistics is given in Table S3 of the Supporting Information. We also analyzed the structures with MolProbity,[23] and the overall score, clash score, and Ramachandran percent favored

dx.doi.org/10.1021/bi500874k | *Biochemistry* 2014, 53, 7582−7595

Table 2. Enzyme Activity of Caspase-3 Allosteric Mutants

	k_{cat} (s^{-1})	K_M (μM)	k_{cat}/K_M (M^{-1} s^{-1})
wild type[a]	0.8	14	5.7×10^4
steric clash			
T140F	0.49 ± 0.03	39 ± 6	1.3×10^4
T140M	(8.6 ± 0.1)x10^{-3}	32 ± 1	2.7×10^2
F55Y	0.03 ± 0.001	13 ± 2	2.3×10^3
F55W	(3.88 ± 0.06) × 10^{-3}	36 ± 3	1.1×10^2
restorative			
T140G/V266H	(2.2 ± 0.5) × 10^{-4}	36 ± 4	6.1×10^0
T140G (control)	1.15 ± 0.04	16 ± 2	7.2×10^4
Y195A/V266H	0.33 ± 0.02	23 ± 3	1.5×10^4
Y195A (control)	0.21 ± 0.007	16 ± 2	1.3×10^4
Y195F/V266H	(8.9 ± 0.7) × 10^{-4}	41 ± 4	2.2 × 10
Y195F (control)	1.18 ± 0.08	28 ± 5	4.2×10^4
M61A/V266H	(1.02 ± 0.03) × 10^{-3}	19 ± 3	5.4 × 10
M61A (control)	1.04 ± 0.05	27 ± 4	3.8×10^4
F128A/V266H	(2.52 ± 0.04) × 10^{-3}	12 ± 1	2.1×10^2
F128A	0.054 ± 0.002	15 ± 2	3.6×10^3
hydrogen bonding			
T140V	0.027 ± 0.002	12 ± 3	2.3×10^3
salt bridge			
K137A	0.98 ± 0.04	17 ± 2	5.8×10^4
E190A	1.24 ± 0.03	18 ± 1	6.9×10^4

[a]From ref 24.

are shown in Table S3 of the Supporting Information. All proteins demonstrated a clash score lower than 10 with the exception of the Y195F/V266H variant. In that case, the clashes fall into three categories: alternate side-chain conformations that impinge on waters associated with the other side-chain conformation, water molecules that are close to charged side chains, and salt bridges between side chains.

Enzyme Activity Assay. The initial velocity was measured in enzyme activity buffer [150 mM Tris-HCl (pH 7.5), 50 mM NaCl, and 1% sucrose] at 25 °C in the presence of varying concentrations of Ac-DEVD-AFC substrate using a BioTek Synergy 2 plate reader, as previously described.[16,24] Final protein concentrations were 10 nM for high-activity mutants and 100 nM for low-activity mutants. Substrate and buffer were mixed in a 96-well plate prior to addition of protein by the plate reader. Samples were excited at 400 nm, and fluorescence emission was monitored at 505 nm for 60 s.

Molecular Dynamics Simulations. Molecular dynamics simulations were performed as previously described.[16] Briefly, simulations were performed for 50 ns with GROMACS 4.5[25] using the Amber99 force field[26] and the TIP3P water model.[27]

Accession Numbers. PDB accession numbers were as follows: caspase-3(F55W) (PDB entry 4QUL), caspase-3(M61A) (PDB entry 4QUG), caspase-3(M61A/V266H) (PDB entry 4QU8), caspase-3(F128A) (PDB entry 4QU9), caspase-3(F128A/V266H) (PDB entry 4QUI), caspase-3-(K137A) (PDB entry 4QUB), caspase-3(T140G) (PDB entry 4QUH), caspase-3(T140G/V266H) (PDB entry 4QUJ), caspase-3(T140F) (PDB entry 4QUD), caspase-3(T140V) (PDB entry 4QU5), caspase-3(E190A) (PDB entry 4QTY), caspase-3(Y195A) (PDB entry 4QTX), caspase-3(Y195A/V266H) (PDB entry 4QU0), caspase-3(Y195F) (PDB entry 4QUA), and caspase-3(Y195F/V266H) (PDB entry 4QUE).

RESULTS

The Enzyme Activity of Restorative Mutants Correlates with the Proximity to H266. Our previous studies of caspase-3(V266H) suggested that relieving steric clashes introduced by H266 should return activity to the enzyme.[16] To test this hypothesis, we introduced mutations at M61, F128, and Y195 in the context of H266, where each amino acid was replaced with alanine. Tyrosine 195 was also replaced with phenylalanine (Table 1 and Figure 2). In addition, we replaced T140 with glycine to introduce a smaller amino acid into helix 3 and disrupt the hydrogen bond with Y195. In the V266H variant,[16] M61 clashes with H121 and disrupts hydrogen bonding between H121 and active site loop 1 (Figure 2c). Surface β-strands 4 and 5 (see Figure 2a) are observed to move relative to their positions in wild-type caspase-3. The movement is exemplified by F128, which forms hydrophobic contacts with M61 and F55 in wild-type caspase-3 (Figure 2c). In the V266H variant, F128 moves closer to the active site, possibly causing M61 to clash with H121. The single mutants M61A, F128A, T140G, Y195A, and Y195F were designed as controls for the restorative double mutants, which have those same mutations in the background of V266H. Data from enzyme activity assays show that the single mutations have little effect on activity (Figure 3a and Table 2). The activity of the F128A variant is the lowest of the control mutants, being reduced 15-fold from that of the wild-type enzyme. Interestingly, the enzyme activity of the Y195F variant is very high, ~75% of the activity of wild-type caspase-3, demonstrating that the through-water hydrogen bond with T140 is not critical for stabilizing helix 3.

All double mutants exhibited some level of activity compared to that of single variant V266H (Figure 3a), which exhibits activity below the detection limit of the assay.[15] Both Y195A and Y195F mutants were made in the context of V266H to determine whether the smaller Y195 to alanine mutation would lead to greater restoration of activity or if it would instead be a change that was too drastic relative to the more conservative change of Y195 to phenylalanine (Figure 2). The Y195A/V266H double mutant demonstrated activity >500-fold higher than that of the Y195F/V266H double mutant, showing that loss of the bulky aromatic ring increases activity when V266 is also replaced with histidine. The increase in activity (k_{cat}/K_M) was reflected in both k_{cat} and K_M parameters, where both parameters were similar to those of the wild-type caspase-3 (Table 2). Indeed, the Y195 to alanine mutation was the most successful in restoring activity, with the Y195A/V266H double mutant having essentially the same activity as the control Y195A single mutant (Table 2 and Figure 3a). In contrast, the activity of the Y195F/V266H variant was ~2600 times lower than that of the wild type, demonstrating that steric clashes introduced by H266 are not relieved by the conservative change of tyrosine to phenylalanine versus tyrosine to alanine. The fact that all of the double mutants gained activity compared to that of the V266H single mutant and the fact that the bulkier Y195F has activity lower than that of the smaller Y195 to alanine substitution again suggest that steric clashes are the primary cause of allosteric inactivation in the V266H mutant. We note that, in general, the changes in activity for the mutants listed in

dx.doi.org/10.1021/bi500874k | Biochemistry 2014, 53, 7582−7595

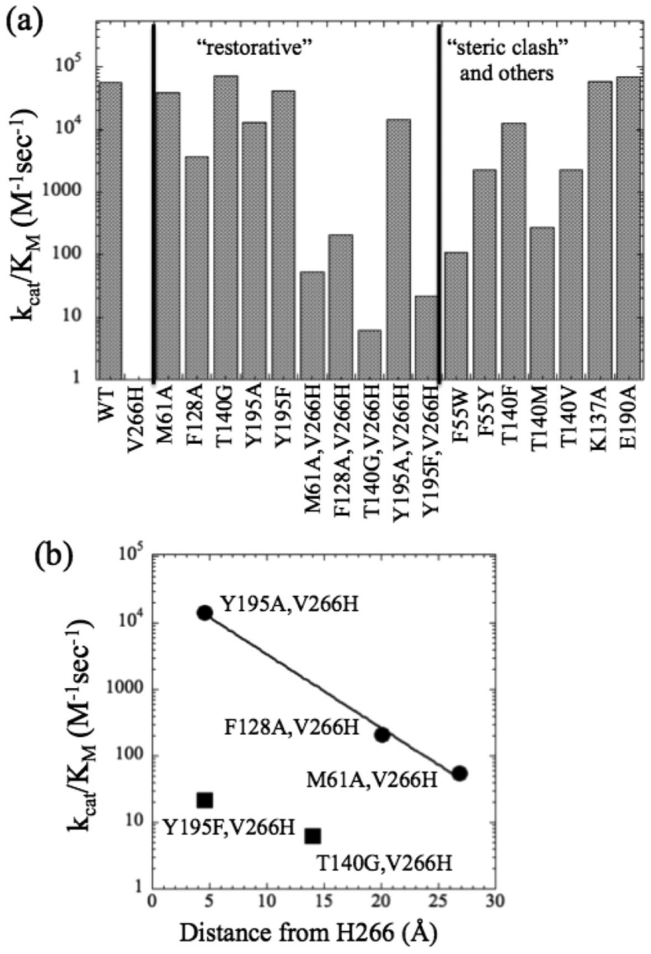

Figure 3. Enzyme activity of wild-type caspase-3 and allosteric mutants. (a) k_{cat}/K_M values for each allosteric mutant. Full steady-state enzyme parameters are listed in Table 2. (b) Comparison of enzyme activity relative to distance from H266, measured from α-carbons. The solid line is present only to show trends in the data.

Table 1 were due to a decrease in k_{cat} values and that mutations that introduced steric clashes also demonstrated increases in K_M. At present, the relationship between the allosteric network and changes in the enzyme catalytic parameters is not known, although both parameters may be affected by changes in the dynamics of active site loops 1 and 3 (substrate-binding loop) as described below.

In helix 3, replacing T140 with glycine was not successful in restoring activity to a significant level in the T140G/V266H double mutant. In contrast, the single mutation, T140 to glycine, had no effect on activity compared to that of the wild-type enzyme (Table 2), indicating that introducing a glycine into the N-terminal region of helix 3 does not affect positioning of the helix. Together, the results for the T140G/V266H and Y195F/V266H double mutants suggest that the new hydrogen bond between Y195 and T140 in the caspase-3(V266H) variant (Figure 2b) is not the cause of the decreased activity in the mutant.

Further from the dimer interface, mutations in the active site of M61 to alanine and F128 to alanine partially restored activity to the V266H variant (Table 2 and Figure 3a). In general, the restoration of activity increased with proximity to H266 (Figure 3b). For the three double mutants (Y195A/V266H, F128A/V266H, and M61A/V266H), the effectiveness of the secondary mutation in alleviating steric clashes introduced by H266 diminishes as the distance from the primary mutation increases. In addition, the Y195 to phenylalanine mutation, as mentioned above, is more bulky than the Y195 to alanine mutation, so its restorative effect is diminished because steric clashes are relieved to a lesser extent (Figure 3b). One outlier in the trend is the T140G/V266H double mutant, which has lower than expected activity. The data show that the steric clashes introduced by H266 are not alleviated by mutations at T140 in helix 3.

It is important to note that the four double mutants with low enzyme activity were not fully processed during expression and purification (Figure S1 of the Supporting Information). In addition, we were unable to fully process the proteins using granzyme B (data not shown). Thus, the activities shown in Figure 3 and Table 2 are likely to represent only the portion of protein that is cleaved. The determination of k_{cat} is dependent on protein concentration, which one assumes to be fully cleaved, so the activity of the cleaved protein is underrepresented and may be higher for these mutants than what is listed in Table 2 because the protein is a mixture of cleaved protein (active) and zymogen (inactive). We also note that the amount of protein that is processed (Figure S1 of the Supporting Information) does not fully account for the low activity of the variants. The activities of the mutants are 2−3 orders of magnitude lower than that of wild-type caspase-3, indicating that the population of cleaved protein also has activity lower than that of the wild-type enzyme.

Restorative Mutants Show Multiple Conformations of H266. We determined the crystal structures for the five restorative mutants as well as the single-mutant controls to greater than 2 Å resolution (Table S3 of the Supporting Information). The structures of all control mutants were very similar to that of wild-type caspase-3, except as noted below, with rmsds of <0.3 Å for all proteins (Table S2 of the Supporting Information); however, the structures of the double mutants showed features of the wild type as well as those of the V266H variant. Wild-type caspase-3 contains six conserved water molecules that H-bond to R164 and R164′ across the dimer interface (see the example in Figure S3a of the Supporting Information). In the case of double mutant Y195F/V266H, four of the conserved central waters were displaced by H266 and H266′, the same as observed in single mutant V266H. The remaining two of the six conserved waters were replaced by cryoprotectant MPD, which H-bonds to the hydroxyl of Y197 (Figure 4a). In addition, H266 is observed in two conformations for one protomer and a single orientation in the second protomer. The side chain of H266 is rotated toward Y197 (and faces R164), or it is rotated toward F195. In the active site of caspase-3(Y195F/V266H), F128 is positioned between that of F128 in the wild-type or V266H structures, and M61 is observed in multiple conformations that limit clashes with H121 (Figure S2a of the Supporting Information).

We performed molecular dynamics simulations for each of the mutants for a total time of 50 ns. The results for caspase-3(Y195F/V266H) show that H266 rotates toward F195 (and H266′ rotates toward F195′) within ∼15 ns, and the histidines remain in that position for the duration of the simulation. Both E124 and E124′ remain inserted into the interface and interact with R164, while K137 is very dynamic and is positioned toward solvent throughout most of the simulation. Interestingly, F195 is significantly more mobile than Y195. With H266 rotated toward F195, the side chain of F195 also rotates toward

dx.doi.org/10.1021/bi500874k | Biochemistry 2014, 53, 7582−7595

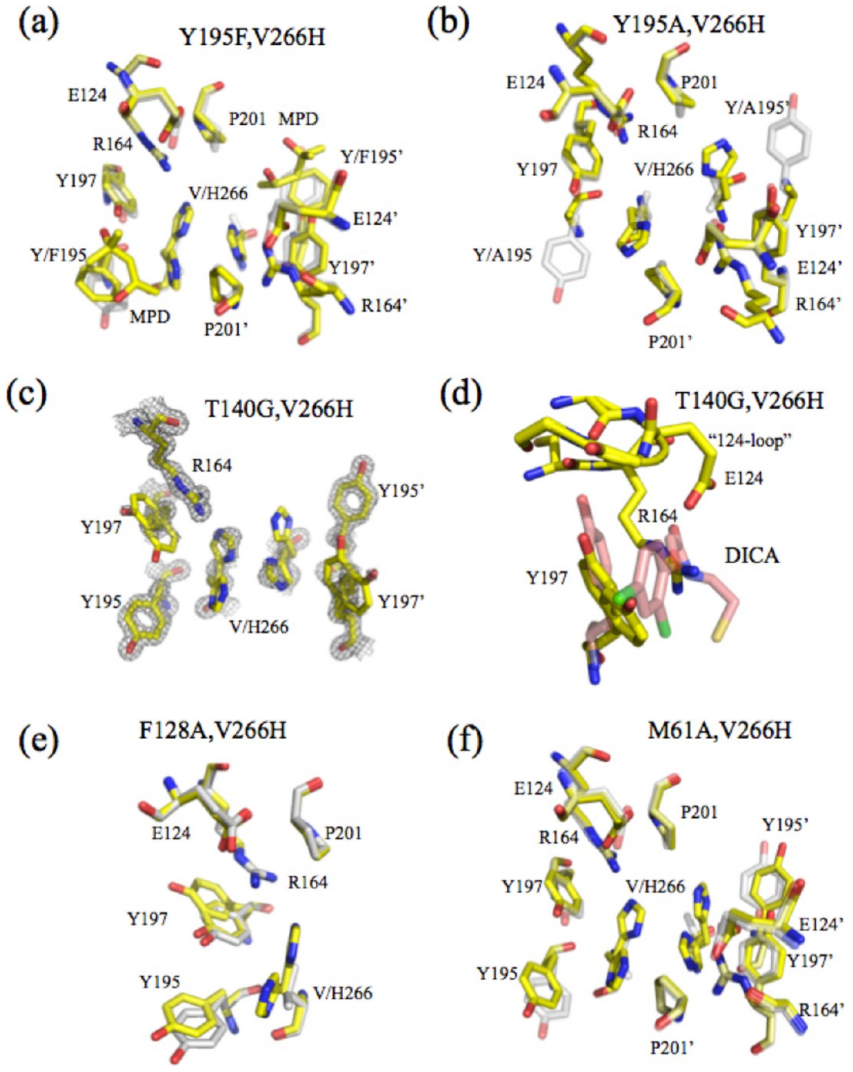

Figure 4. Structures of restorative mutants. Dimer interface of (a) Y195F/V266H, (b) Y195A/V266H, (c and d) T140G/V266H, (e) F128A/V266H, and (f) M61A/V266H. For panels a–f, amino acids are colored yellow for the mutant and gray for WT caspase-3. In panel c, electron density is shown by black mesh. In panel d, the position of Y197 is compared to that of caspase-7 with an allosteric inhibitor, DICA, bound (pink, PDB entry 1SHJ).

β-strand 6, which is not observed for Y195 in wild-type caspase-3 (compare panels a and b of Figure 5). In the active site of caspase-3(Y195F/V266H), H121 rotates toward C163 within the first ~15 ns and remains in that position for the remainder of the simulation. Following the rotation of H121, M61 moves behind H121 (toward solvent) and prevents it from rotating back toward active site loop 1 (see the example in Figure 5e). These movements are observed in one of the two active sites in wild-type caspase-3, where the distance between T62 and H121 fluctuates between ~6 and ~9 Å. In the second active site of wild-type caspase-3, the distance is constant at ~3 Å, demonstrating that the hydrogen bond between T62 and H121 is maintained during the time course of the simulation. A comparison of the distances in wild-type caspase-3 and the M61A/V266H double mutant (as an example) is shown in Figure S7 of the Supporting Information (panels a and b).

In contrast to the Y195F variant, the structure of caspase-3(Y195A/V266H) demonstrates a single orientation for H266 (Figure 4b), which is observed to orient toward A195 and away from R164. Likewise, H266′ is oriented toward A195′ and away from R164′. Like caspase-3(Y195F/V266H), the six conserved waters are missing from the interface. For this variant, however, the active site residues more closely resemble their positions in wild-type caspase-3 versus the V266H variant (Figure S2b of the Supporting Information). From MD simulations, one observes that H266 does not fluctuate from the original position; that is, it does not rotate toward R164 (Figure 5c). Although the salt bridge between K137 and E190 is observed in the crystal structure, the MD simulations show that the interactions are transient, because K137 appears to be dynamic and is exposed to solvent throughout much of the simulation (data not shown). Also in contrast to the Y195F variant, the position of H121 mostly remains in close contact with loop 1, similar to that observed for wild-type caspase-3 (see the example in Figure 7b of the Supporting Information). As a result, loop 1 is less mobile, and M61 does not move toward H121.

Although the activity of single mutant T140G is the same as that of wild-type caspase-3 (Table 2 and Figure 3a), double mutant T140G/V266H regained only modest activity compared to that of single mutant V266H. As with the other H266 variants, four of the six central water molecules are displaced by

dx.doi.org/10.1021/bi500874k | *Biochemistry* 2014, 53, 7582–7595

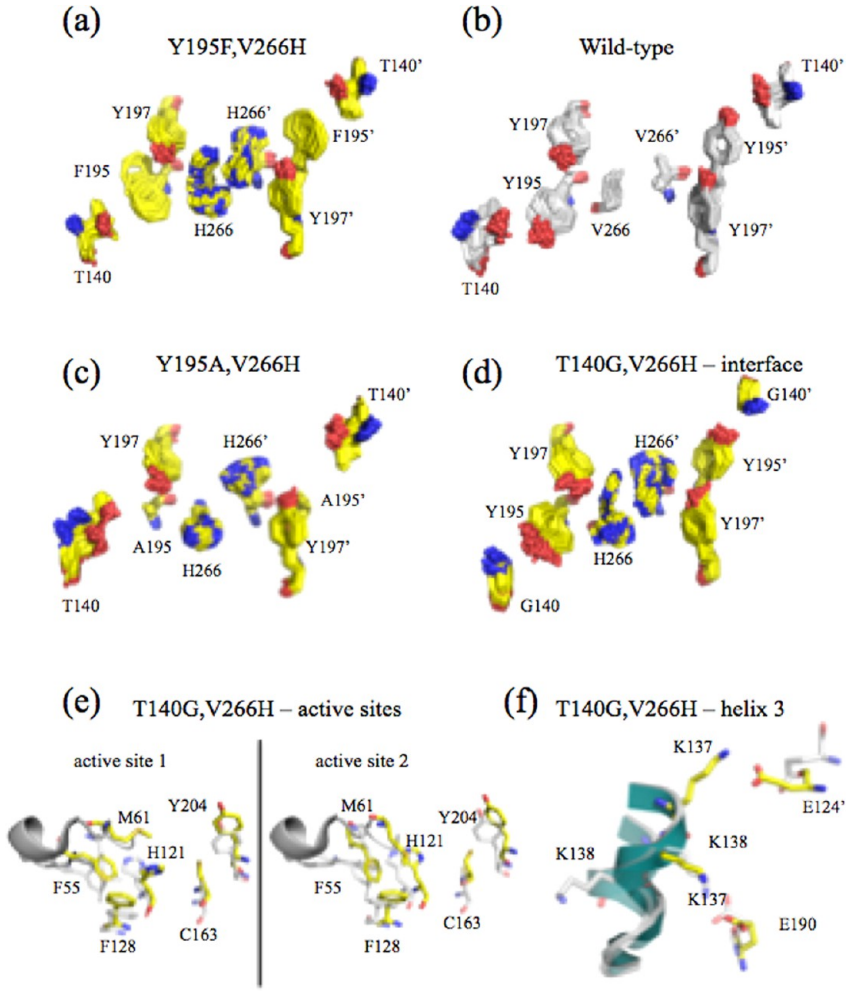

Figure 5. Molecular dynamics simulations of interface restorative mutants. MD simulations of (a) Y195F/V266H, (b) wild type, (c) Y195A/V266H, and (d–f) T140G/V266H. Panels a–d show 200 frames (at 250 ps intervals) of the 50 ns simulation to demonstrate movements of the amino acids in the dimer interface. (e) Active site residues for T140G/V266H at time zero (gray) and 29 ns (yellow). (f) Position of helix 3 at time zero (gray) and 24 ns (yellow).

H266 and two water molecules are replaced by DTT molecules. The DTTs H-bond with Y197 (Figure 4c). The side chain of Y195 is observed in the same position as in the V266H variant, but in this case, it forms a H-bond with N141 in helix 3 through two water molecules (see the example in Figure S5b of the Supporting Information). In addition, the active site residues align closely with those of wild-type caspase-3 (Figure S2c of the Supporting Information). Interestingly, the side chain of Y197 is observed in two conformations (Figure 4c). While one conformation is the same as that in wild-type caspase-3, the second orientation is similar to that observed upon binding of the allosteric inhibitor DICA (Figure 4d).[6] In contrast to caspase with an allosteric inhibitor bound, however, the substrate-binding loop (L3) is intact in the T140G/V266H variant, so R164 is intercalated between Y197 and P201, that is, in the active conformation. In the alternate orientation, Y197 H-bonds with two water molecules that contribute to a H-bond network in the "124 loop" (contains E124), including backbone atoms of I126, E123, C163, and G125 and the side chains of E124 and R164 (data not shown).

Results from MD simulations for the T140G/V266H double mutant show that H266 rotates toward Y195, although it appears to fluctuate between the two conformations (Figure 5d). Interestingly, the position of Y197 is similar to that of wild-type caspase-3, so the second orientation observed in the crystal structure is not observed in the MD simulations. The side chain of Y195 shows higher mobility than it does in wild-type caspase-3, similar to that of F195 in the Y195F/V266H variant (Figure 5a). In one active site, the side chain of H121 rotates toward C163, similar to that described above for the Y195F/V266H variant (Figure 5e, left panel). Following the rotation of H121, M61 rotates toward solvent and prevents H121 from rotating back to its starting position, as described above. In the second active site, H121 remains in its original position, similar to that observed for wild-type caspase-3 (Figure 5e, right panel). Importantly, helix 3 is stable in one protomer, but in the second protomer, the N-terminus of helix 3 rotates toward the dimer interface (Figure 5f). In this orientation, K137 (helix 3) no longer interacts with E190 but rather interacts transiently with E124′ across the dimer interface. In addition, K138 (helix 3) rotates toward E190. These movements were observed for single mutant V266H,[16] so combining the T140G mutation with H266 does not prevent helix 3 from sampling the inactive conformation. Overall, the data for this double mutant show that the active site H121 catalytic group can be characterized with intermediate mobility, fluctuating between two conformations, and helix 3 remains destabilized.

dx.doi.org/10.1021/bi500874k | *Biochemistry* 2014, 53, 7582–7595

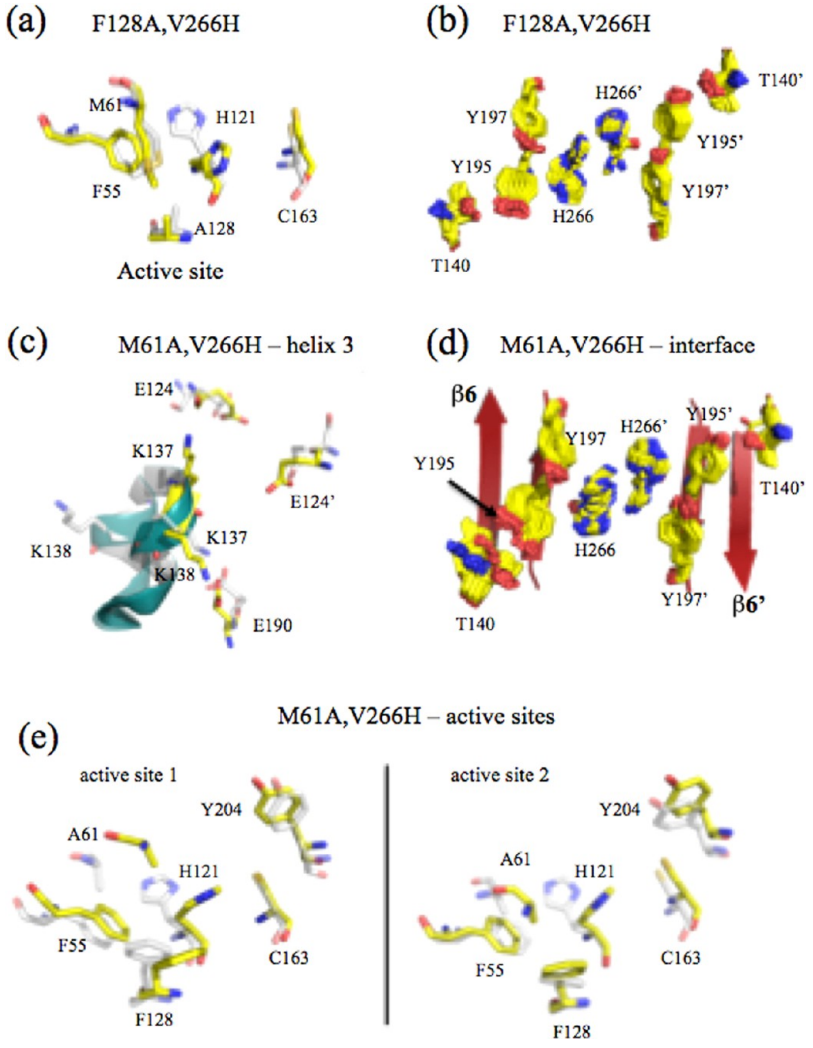

Figure 6. Molecular dynamics simulations of active site restorative mutants. MD simulations of (a and b) F128A/V266H and (c and d) M61A/V266H. (a) Comparison of active site residues for F128A/V266H at time zero (gray) and 18 ns (yellow) demonstrates movement of H121 toward C163. (b) Two hundred frames (at 250 ps intervals) of the 50 ns simulation for F128A/V266H demonstrate movements of the amino acids in the dimer interface. (c) The position of helix 3 is shown at time zero (gray) and 50 ns (yellow) for M61A/V266H. (d) Two hundred frames (at 250 ps intervals) of the 50 ns simulation for M61A/V266H demonstrate movements of the amino acids in the dimer interface. (e) Comparison of active sites of M61A/V266H at time zero (gray) and 50 ns (yellow) demonstrate movement of H121 toward C163.

As described above, the single mutation of F128 to alanine resulted in a decrease in k_{cat} of ~15-fold (Table 2). The structure of the F128A variant demonstrated a dimer interface (Figure S2c of the Supporting Information) and active sites (Figure S2d of the Supporting Information) very close to those of wild-type caspase-3. We note, however, the presence of a DTT molecule at the site of the mutation in the single mutant, although no DTT molecules were observed in the active site of the double mutant. Overall, there were no major structural perturbations due to the mutation. MD simulations of the single mutant demonstrate that loop 1 appeared to be less mobile than that of wild-type caspase-3 due to replacement of F128 on β-strand 4. Thus, double mutant F128A/V266H exhibited activity only ~20-fold lower than that of the F128A single variant. The X-ray crystal structure of the double mutant shows that H266 is observed in two orientations (Figure 4e), similar to that described for Y195F/V266H (Figure 4a) and T140G/V266H (Figure 4c). In addition, Y195 is observed in the same orientation as in the V266H single mutant; that is, it H-bonds directly with T140. Interestingly, Y197 is observed in two orientations, as described above for the T140G/V266H double mutant (compare panels c and e of Figure 4). The second orientation of Y197 has the same H-bonding network as in T140G/V266H. Like single variant F128A, the active site residues are not perturbed by the mutation (Figure S2d of the Supporting Information).

Results from MD simulations for the double mutant (F128A/V266H) show that, as described above, H266 moves toward Y195 and remains in this position throughout the simulation (Figure 6b). Elsewhere in the dimer interface, E124 remains inserted and close to R164, so it is not available to interact with K137′ across the interface. In addition, the distance between the hydroxyl groups of Y195 and T140 fluctuates between 2.5 and 3.3 Å, so the H-bond appears to be stable. Importantly, helix 3 is also stable; that is, it does not rotate toward the interface as described for the T140G/V266H variant (Figure 5f). Like the single mutant (F128A), M61 does not block H121 but rather remains near F55 and A128 (Figure 6b). For this mutant, the MD simulations suggest that the presence of F128 on β-strand 4 is important for maintaining

dx.doi.org/10.1021/bi500874k | *Biochemistry* 2014, 53, 7582−7595

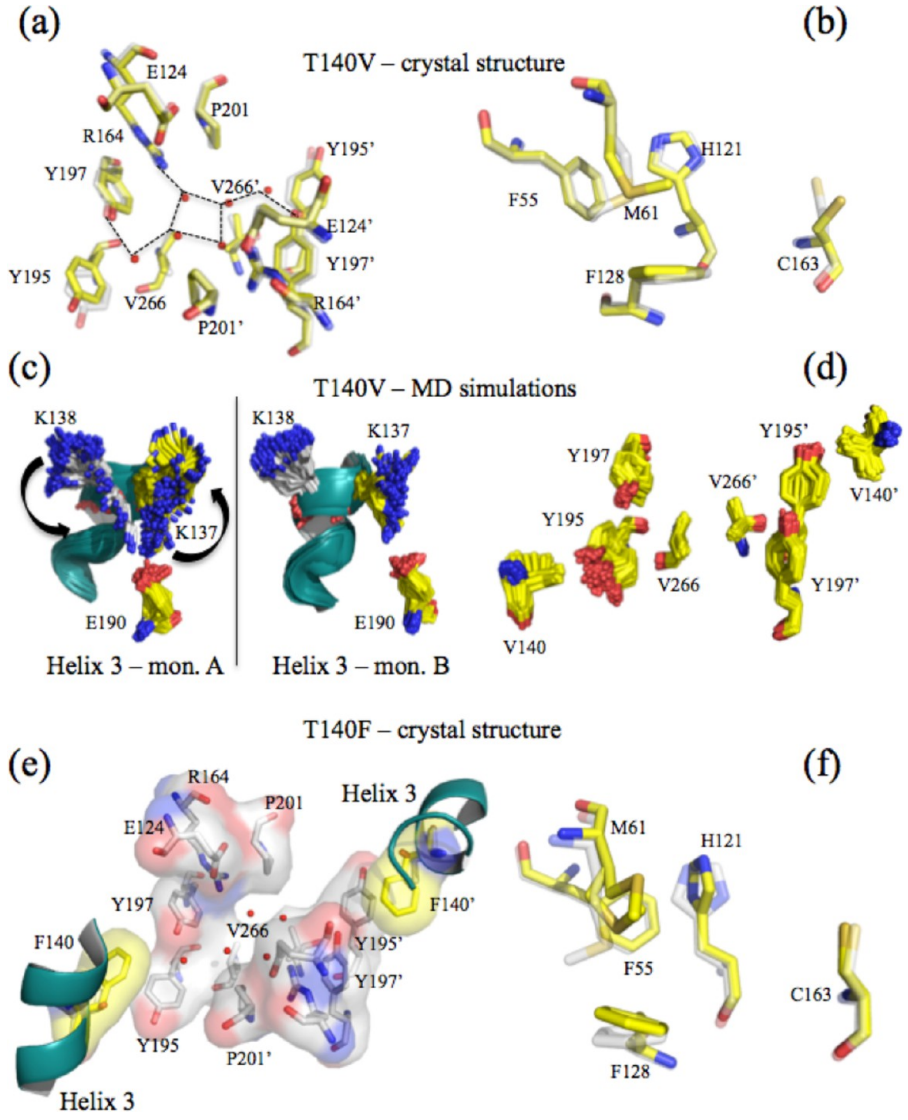

Figure 7. Comparison of helix 3 mutants. (a and b) Crystal structure of T140V comparing the dimer interface (a) and active site (b) with WT. Amino acids are colored yellow for the mutant and gray for WT caspase-3. Red spheres represent conserved water molecules in the interface, and the dashed lines represent the H-bonding network. (c and d) MD simulations of T140V. Two hundred frames (at 250 ps intervals) of the 50 ns simulation demonstrate movements of the amino acids in helix 3 (c) (left panel, protomer A; right panel, protomer B) and the dimer interface (d). For the sake of clarity, K138 is colored gray and blue while K137 is colored yellow and blue (c). Dimer interface (e) and active site (f) of T140F. In panel e, red spheres represent conserved water molecules in the interface. For panel f, amino acids are colored yellow for the mutant and gray for WT caspase-3.

optimal flexibility in active site loop 1. A decreased flexibility in loop 1 may correlate with the decrease in k_{cat} for the single and double mutants.

The M61A single variant displayed enzyme activity very similar to that of wild-type caspase-3 (Table 2), and the structure overlaid very closely with that of wild-type caspase-3 (Table S2 of the Supporting Information). At the site of the mutation, the side chain of F128 is observed to move toward the cavity produced by replacing M61 with alanine (Figure S3b of the Supporting Information), while no other changes are observed in the active site. Like the T140G/V266H double mutant described above, the M61A/V266H double mutant also had very low activity (Table 2). The crystal structure of the double mutant shows that the salt bridge between K137 and E190 is intact, as in wild-type caspase-3, and that H266 resides in two conformations (Figure 4f), as described above for Y195F/V266H (Figure 4a), T140G/V266H (Figure 4c), and F128A/V266H (Figure 4e) variants. One observes that Y195 retains the direct H-bond with T140, as in the V266H single mutant. In addition, F128 moves toward the cavity generated by the M61 to alanine mutation, as observed in the M61A single mutant (Figure S2e of the Supporting Information). Molecular dynamics simulations of the double mutant show that, as observed in the V266H single mutant, K137 interacts with E124′ across the dimer interface, and the N-terminus of helix 3 rotates toward the interface so that K138 interacts with E190 (Figure 6c). The data show that replacing M61 with alanine does not relieve the effects of H266 on destabilizing helix 3. Elsewhere in the interface, the rotation of helix 3 toward the dimer interface disrupts interactions between Y195 and T140 because T140 rotates toward the surface, so Y195 is observed to move further toward β-strand 6 (Figure 6d). In addition, H266 samples both conformations observed in the crystal structure, in contrast to mutants described above where

dx.doi.org/10.1021/bi500874k | *Biochemistry* 2014, 53, 7582−7595

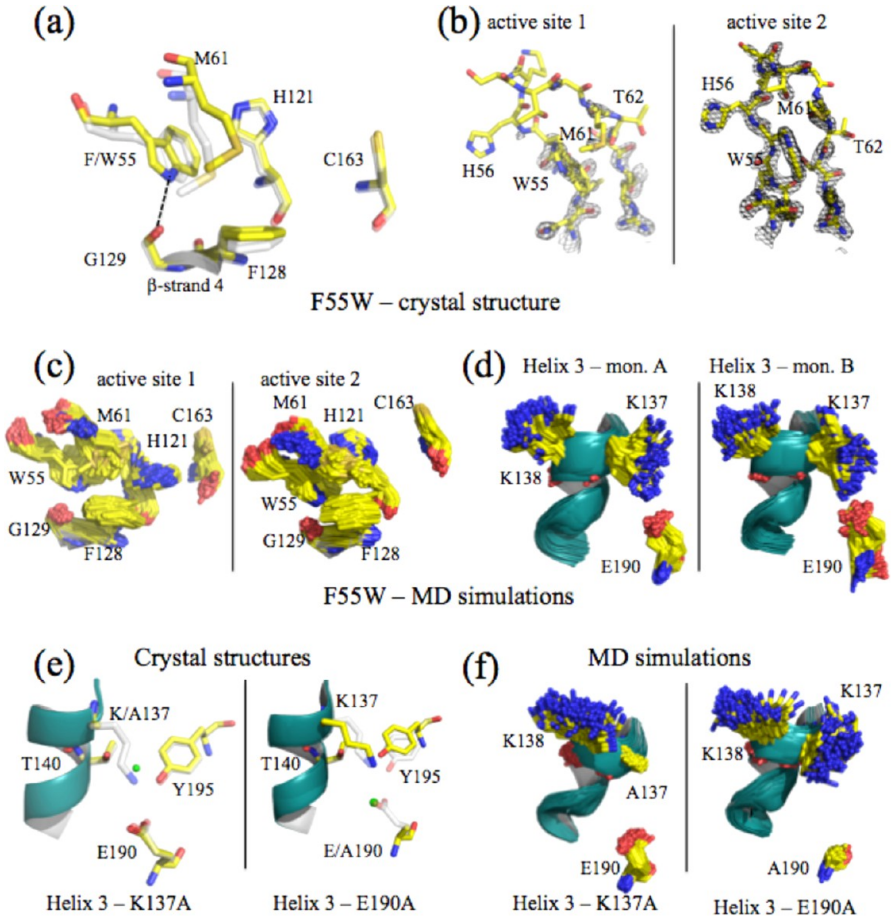

Figure 8. Structures and MD simulations of steric clash and salt bridge mutants. Comparison of active site residues (a) and of active site loop 1 (b) from the crystal structure of F55W. In panel a, amino acids are colored yellow for the mutant and gray for WT caspase-3. The new hydrogen bond between W55 and G129 is shown by the dashed line. In panel b, a lack of electron density (black mesh) in active site 1 shows disorder in several residues of loop 1 (left), whereas the loop is well ordered in the second active site (right). MD simulations show movements in the active site residues (c) and helix 3 (d) of F55W. (e and f) Comparison of helix 3 for K137A (left) and E190A (right) from the crystal structures (e) or from MD simulations (f). In panel e, the green sphere represents a new water molecule observed in the mutants. Amino acids are colored yellow for the mutant and gray for WT caspase-3. For panels c, d, and f, 200 frames (at 250 ps intervals) of the 50 ns simulations are shown to demonstrate movements of the amino acids.

H266 rotates toward Y195 and remains in that position. In one active site, A61 fluctuates toward a solvent-exposed position behind H121 (Figure 6e, left panel), whereas in the second active site, A61 remains in the starting position, interacting with F55 and F128 (Figure 6e, right panel). One striking observation from the MD simulations is that the movement of helix 3 toward the dimer interface results in an ~7 Å decrease in distance between the two active sites. The distance between loop 1 and loop 1′ decreases from ~42 to ~35 Å, which is due to the rotation of helix 3 and movements of surface β-strands 4 and 5, as well as both loops, toward the interface. In wild-type caspase-3, the distance fluctuates between 40 and 42 Å over the course of the simulation (Figure S7c of the Supporting Information).

Overall for the restorative mutants, a destabilized helix 3 was observed in the V266H single mutant, but no rotation in the helix was observed in the F128A/V266H, Y195A/V266H, and Y195F/V266H double mutants. We consider those three mutations to have a stabilizing effect on helix 3 in the context of H266. The M61A/V266H and T140G/V266H mutants (which have low activity), on the other hand, showed a destabilized helix 3 similar to that of the V266H single mutant. Therefore, removal of steric clashes introduced by H266 and stabilization of helix 3 are correlated with higher activity, whereas retaining the steric clashes (Y195F/V266H, for example) and destabilization of helix 3 are correlated with lower activity.

Introduced Steric Clashes Mimic the Inactive V266H Mutant and Have Activity That Is Decreased Relative to That of the Wild-Type Enzyme. We chose two sites in caspase-3, T140 and F55, located in helix 3 and loop 1, respectively (Figure 2a), to introduce steric clashes. The rationale for these two sites is based on the data described above for the restorative mutants. T140 is located in helix 3 and is close to the region that is destabilized in the V266H variant (Figure 2b), while F55 is located in active site loop 1 and forms a hydrophobic cluster with F128 (β-strand 4) and M61 (loop 1) (Figure 2c). Our goal was to determine whether steric clashes elsewhere in the allosteric network could mimic the effects of H266. In this regard, we examined mutations of T140 to valine, methionine, or phenylalanine and mutations of F55 to tyrosine or tryptophan. The T140V variant removes H-bonding ability with Y195, while T140M and T140F increase the size of the side chain. Likewise, the Y55 mutation introduces a hydroxyl group into the aromatic ring while the mutation to

dx.doi.org/10.1021/bi500874k | *Biochemistry* 2014, 53, 7582−7595

tryptophan increases the side-chain volume by 38 Å^3 compared to that with phenylalanine.

Enzyme activity assays show that removal of the H-bond with Y195 using the isosteric side-chain valine to replace T140 decreased activity ~25-fold (Table 2 and Figure 3a). The effects were not equivalent to those of the Y195F single mutant described above (1.4-fold decrease), so the presence of V140 may also affect helix 3 in addition to removing the H-bond with Y195. At present, however, it is not clear from the activity data why mutations at the two sites are not equivalent. Increasing the size of the side chain to that of methionine resulted in a ~200-fold decrease in activity, while the T140F mutant decreased activity only ~4-fold. In the active site, increasing the size of the side chain at position 55 had large effects on activity (Table 2 and Figure 3a). The F55Y variant demonstrated ~25-fold lower activity than wild-type caspase-3, and the activity of the F55W variant was ~500-fold lower than that of wild-type caspase-3.

The crystal structure of the T140V variant shows that the six conserved water molecules are present in the dimer interface, as with wild-type caspase-3 (Figure 7a). The side chain of Y195 is shifted somewhat toward helix 3, but it is closer to the position observed in wild-type caspase-3 than that of the V266H variant. At the site of the mutation, helix 3 overlays well with the comparable helix in wild-type caspase-3. The salt bridge between K137 and E190 is intact, but a through-water H-bond between Y195 and T140 is missing in the mutant (data not shown). In the active site, the side chain of M61 is rotated so that the terminal CH_3 is oriented toward solvent, but F128, F55, H121, and C163 overlay well with the wild-type active site (Figure 7b). Molecular dynamics simulations of this mutant show that K137 is very mobile on one side of the interface, while K137′ is less mobile and remains close to E190 for longer times (data not shown). Helix 3 is less stable than observed in wild-type caspase-3 but does not fully undergo the transition to the inactive conformation (Figure 7c). Although K137 interacts with the carbonyl of P201′ across the interface and K138 rotates toward E190, the movements are transient such that the helical structure is mostly favored. During the helix fluctuation, the side chain of Y195 rotates approximately 90°, although the hydroxyl retains its orientation toward helix 3 (Figure 7d).

The structure of the T140F variant shows that the dimer interface overlays very closely with that of wild-type caspase-3 (Figure S6a of the Supporting Information), and five of the six conserved water molecules are retained in this variant (Figure 7e). Interestingly, the side chain of F140 fills a cavity at the base of the dimer interface, without causing movements in surrounding amino acids, and interacts with Y195 through π-stacking interactions (Figure 7e). Molecular dynamics simulations also show little movement in the interface or at the site of the mutation (Figure S6b of the Supporting Information). Importantly, helix 3 remains in the position of the active conformation. In the active site, F128 moves closer to M61, which is oriented toward solvent as described above for the T140V variant (Figure 7f). In addition, H121 remains positioned toward loop 1, but the side chain is rotated approximately 90°. MD simulations show that, in one active site, M61 rotates toward solvent even though H121 remains in the orientation that faces loop 1. In the second active site, however, H121 also rotates to face C163 (Figure S6c of the Supporting Information). We also note that C163 is quite dynamic in both active sites and fluctuates between orientations close to substrate and facing loop 2 (Figure S6c of the Supporting Information).

The enzyme activity data showed that increasing the size of the side chain at position 55 in loop 1 correlated with a decrease in activity (Table 2). Unfortunately, we are unable to report the structure of the F55Y variant, but we determined the structure of F55W to 1.9 Å resolution (Table S3 of the Supporting Information). The active site groups overlay well with those of wild-type caspase-3 with the exception of M61, which is displaced because of the large tryptophan side chain. In addition, the indole nitrogen forms a new H-bond with the carbonyl of G129, which resides on a turn between β-strands 4 and 5 (Figure 8a). While the electron density is good for W55 in both active sites, several residues in loop 1 (H56−T62) are disordered in one active site, indicating that the H-bond between the catalytic H121 and the backbone carbonyl of T62 is disrupted (Figure 8b). In the interface, the six conserved water molecules are present in the mutant, and the interface overlays very closely with that of wild-type caspase-3 (Figure S6d of the Supporting Information). MD simulations of the F55W variant show that the H-bond between W55 and G129 is maintained throughout the simulation, resulting in a lower mobility of M61 (Figure 8c). In one active site, the side chain of H121 rotates toward C163, as described above for other mutants (Figure 8c, left panel). In the second active site, however, H121 remains H-bonded to the carbonyl of T62 in loop 1; that is, it does not rotate toward C163 (Figure 8c, right panel). In both active sites, M61 remains in close contact with the hydrophobic cluster of F128 and W55 (Figure 8C). Finally, there are no major changes in the dimer interface (Figure S6d of the Supporting Information), and helix 3 remains stable, as shown by the lack of rotation in K137 and K138 (Figure 8d).

Overall, the steric clash mutants show that one can effectively mimic the effects of H266 by introducing steric clashes at other sites in the allosteric network. The data further support the notion that the stability of helix 3 is important for maintaining the active state within the native ensemble. Likewise, the mobility of loop 1, possibly in combination with maintaining the H-bond between H121 and T62, appears to affect activity, particularly with regard to movement of M61 to a solvent-exposed position when H121 rotates toward C163. Either destabilizing helix 3, changing the mobility of loop 1, or both results in a decrease in activity.

The K137−E190 Salt Bridge Is Transient and Has No Effect on Activity. The E190A and K137A mutants were designed to test the importance of a salt bridge between K137 in helix 3 and E190 in the dimer interface (Figure 2b). Although this salt bridge is present in wild-type caspase-3, it is disrupted in the inactive V266H mutant, where K137 is exposed to solvent.[16] This movement of K137 is likely due to distortion of the N-terminus of helix 3, as described above. On the basis of the structure of the V266H variant, we suggested that the movement of K137 could affect residues across the interface to destabilize the L2−L2′ loop bundle, which has been shown to stabilize the active site.[17] Unexpectedly, both the E190A and K137A mutants had full enzymatic activity (Figure 3a and Table 2), demonstrating that the salt bridge between E190 and K137 is unnecessary for catalysis.

The structures of the E190A and K137A variants differ very little from that of wild-type caspase-3, where one observes that the interfaces (Figure S6e of the Supporting Information) and the active sites (Figure S6f of the Supporting Information) overlay very closely with those of wild-type caspase-3. A new

dx.doi.org/10.1021/bi500874k | Biochemistry 2014, 53, 7582−7595

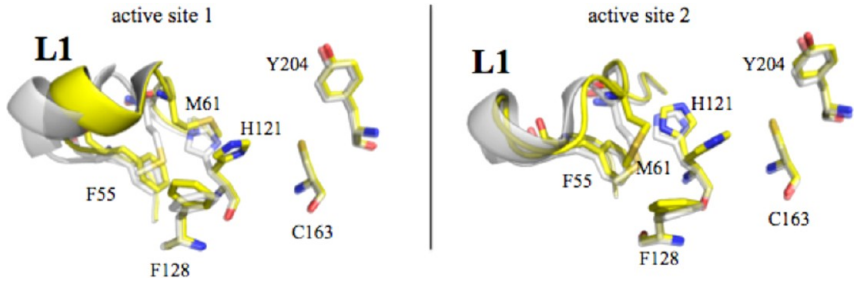

Figure 9. Comparison of the positions of H121 and M61 in wild-type caspase-3. X-ray crystal structures of wild-type caspase-3 with Ac-DEVD-CMK inhibitor (gray) (PDB entry 2J30) or Ac-LDESD-CHO inhibitor (yellow) (PDB entry 3EDQ). The structure with a pentapeptide inhibitor demonstrates two positions for H121 in both active sites. In addition, in active site 1, M61 is positioned toward solvent and blocks rotation of H121 toward loop 1. In active site 2, M61 retains contacts with the hydrophobic cluster of F55 and F128. Similar conformations are observed for M61 and H121 in molecular dynamics simulations of caspase-3 variants, as described in the text.

water molecule is in place of the side chains in both variants (Figure 8e), and the remaining hydrogen bonding network connects N141 of helix 3 to E190. The molecular dynamics simulations for all of the mutants described above show that the salt bridge between K137 and E190 is transient, which is consistent with the observation that mutating either of the residues does not decrease the activity of the enzyme. The crystal structure of the E190A variant shows that Y195 retains a direct H-bond with T140 of helix 3 (Figure 8e, right panel), and MD simulations show that the distance between the hydroxyl of Y195 and T140 fluctuates between 2.8 and 4.1 Å. Importantly, helix 3 is stable in both mutants. Overall, the data for the K137A and E190A variants show that removing the salt bridge results in localized changes in the structure that have no effect on the interface, helix 3, or the active sites, so there is no decrease in enzyme activity.

■ DISCUSSION

We have shown that mutations in the context of H266 restore activity by relieving steric clashes caused by placing a histidine in the center of the dimer interface. The secondary mutations are most effective when placed close to H266. Structural studies show that the mutations affect the position of H266, which rotates toward either Y197 or Y195, on opposite ends of β-strand 8. The data are consistent with our previous studies in which we showed that replacing E124 with alanine (E124A/V266H) also resulted in two conformations of H266.[16] Molecular dynamics simulations of the mutants show that the orientation of H266 toward Y195 predominates (see Figure 5c, for example), possibly because Y195 has greater mobility in the cavity than does Y197 and thus can more easily accommodate the bulky histidine residue. The mobility of Y195 within the allosteric site has been described previously.[16]

The movement of the N-terminus of helix 3 toward the dimer interface is characterized by an apparent rigid-body translation and rotation toward the dimer interface, effectively decreasing the volume of the central cavity of the dimer interface by ~800 Å^3 (from 1750 to 950 Å^3).[16] In addition, the mobility of active site loop 1 is increased in caspase-3(V266H), and the S1′ binding pocket is narrower. The restorative mutants in the context of H266 stabilize helix 3 such that the native helix is favored over the inactive state. Furthermore, molecular dynamics simulations showed that mutations closest to H266, such as Y195A, had the greatest effects on preventing the rotation of helix 3. In contrast, mutations at greater distances, for example, M61A, were less effective in influencing the position of helix 3. The data are consistent with the notion that helix 3 samples two conformations within the native ensemble. In the active conformer, helix 3 is fully formed, while in the inactive conformer, the amino terminus of helix 3 rotates toward the dimer interface, resulting in a shorter distance between the two active sites and a smaller cavity in the dimer interface. The activity of the enzyme reflects the relative population of each conformation within the native ensemble.

The steric clash mutants decreased activity by either affecting the position of helix 3, affecting the mobility of loop 1, or both. For example, increasing the size of the side chain at position 55 in active site loop 1 from phenylalanine to tyrosine to tryptophan results in a progressive decrease in enzyme activity. Although we were unable to report the crystal structure of the F55Y variant, the structure of F55W shows a new hydrogen bond with β-strand 4, and MD simulations show that the H-bond is stable throughout the simulation, resulting in a lower mobility of loop 1.

A consistent theme in the caspase-3 mutants described here is the transient rotation of the catalytic H121 toward C163. Along with this rotation, M61, and loop 1 in general, rotates toward active site loop 4. The movement results in positioning M61 toward solvent, which prevents H121 from returning to its starting position, that is, hydrogen-bonded with T62. We note that the conformations of H121 and of M61 shown in our MD simulations were also observed in structural studies of caspase-3 bound to the pentapeptide inhibitor, Ac-LDESD-CHO (Figure 9). Weber and colleagues showed crystallographic evidence of M61 rotated toward solvent,[28] where M61 occupies the position of H121 if it were H-bonded to T62. Thus, H121 cannot rotate toward T62 unless M61 rotates toward the hydrophobic cluster of F55 and F128. The movements of H121 have been suggested to be important for the catalytic mechanism of caspases,[29] and our data suggest that the movement is coordinated with mobility in loop 1. The data from MD simulations presented here for the allosteric mutants at positions 55 and 128 show a change in mobility of active site loop 1, suggesting that the loop dynamics are critical for maximal enzyme activity. Changing the mobility of loop 1, either increasing or decreasing mobility, results in a lower activity. The conclusions are consistent with structural studies of other caspases, where it is well-known that caspases are inhibited through conformational changes in loop 1. For example, in the zymogen of caspase-8, loop 1 is locked in the active site cleft through interactions with the intersubunit linker.[30] A similar orientation was suggested for caspase-3 inhibited by calbindin-D28K, where two helices in the EF-hand 1 region lock loop 1 in the substrate-binding cleft.[31] Likewise,

dx.doi.org/10.1021/bi500874k | *Biochemistry* 2014, 53, 7582−7595

high mobility is suggested by the disorder of loop 1 in recently described structures of procaspase-3.[32]

Mutations in helix 3 showed that the new H-bond between T140 and Y195 observed in caspase-3(V266H) is not the cause of inactivation. We removed the hydrogen bonding potential of T140 and of Y195, and the T140G/V266H and Y195F/V266H mutants remained inactive. In both cases, helix 3 remained destabilized. Removing the hydroxyl group of T140 also resulted in a destabilized helix 3. For example, the T140V single mutant demonstrated a 25-fold decrease in activity, and MD simulations showed that, while the native helix was favored, the inactive conformation was sampled by the variant. Although we were unable to determine the crystal structure of the T140M variant, we infer that the low activity of the mutant is also due to increased mobility in helix 3. Thus, removing the hydroxyl group of T140 appears to lower the free energy barrier between the fully formed (active) and rotated (inactive) helix, and the lower enzyme activity reflects the increase in the extent of sampling of the inactive conformation. We previously showed that a double mutant in the allosteric site, E124A/Y197C, resulted in a decreased activity and a destabilized helix 3,[16] which is consistent with the effects on helix 3 described here. Collectively, our data show that sites other than V266 can induce similar effects by destabilizing helix 3, affecting the mobility of loop 1, or both.

Helix 3 has been shown to be important in allosteric regulation of other caspases. In caspase-6, for example, the binding of zinc to an allosteric site results in an extended conformation of helix 3, where β-strands 4 and 5 undergo a sheet-to-helix transition.[33] The extended helix 3 also affects the positions of the adjacent helix 2 and active site loop 1, so the enzyme is catalytically inactive. Furthermore, at the C-terminal end of helix 3, in a loop connecting the helix to β-strand 6, S150 is phosphorylated by p38-MAPK, an event reported to inhibit caspase-3 and prevent Fas-mediated apoptosis in neutrophils.[34] The site is also conserved in caspase-8.[35] Similarly, caspase-6 is phosphorylated by ARK5 at S257, resulting in a zymogen-like structure.[36,37] On the basis of our data for allosteric regulation of caspase-3, particularly the role of helix 3 in allostery, we speculate that phosphorylation of the loop C-terminal to helix 3 destabilizes the helix in a manner described here for the caspase-3 variants.

Studies of caspase-3 inhibition have focused on activity-based probes targeting the active site[38,39] or on allosteric inhibitors that bind to the dimer interface and cause a conformational shift to a structure similar to that of the inactive zymogen, where the active site loops are disordered (see Figure 1).[6] Our data show the presence of additional inactive conformations in which the active site remains mostly intact, particularly the substrate-binding loop, but a region of helix 3 is destabilized and rotates toward the dimer interface. Targeting the inactive state within the native ensemble may also provide additional probes for allosteric inhibition. Such inhibitors would be expected to be highly specific and would depend on the stability of helix 3 in the various caspases.

■ ASSOCIATED CONTENT

Supporting Information

A sodium dodecyl sulfate−polyacrylamide gel electrophoresis gel of several mutants with low intrinsic processing, five figures that further describe the active sites and dimer interfaces of the allosteric variants, one figure that summarizes distance calculations from molecular dynamics simulations, one table that lists oligonucleotide primers used for site-directed mutagenesis, one table listing the rmsds of allosteric variants compared to wild-type caspase-3, and one table that summarizes the X-ray crystallography data collection and refinement statistics. This material is available free of charge via the Internet at http://pubs.acs.org.

■ AUTHOR INFORMATION

Corresponding Author

*Department of Molecular and Structural Biochemistry, 128 Polk Hall, North Carolina State University, Raleigh, NC 27695-7622. E-mail: clay_clark@ncsu.edu. Phone: (919) 515-5805. Fax: (919) 515-2047.

Funding

This work was supported by National Institutes of Health Grant GM065970 to A.C.C.

Notes

The authors declare no competing financial interest.

■ ACKNOWLEDGMENTS

We thank the research agencies of North Carolina State University and the North Carolina Agricultural Research Service. Use of the Advanced Photon Source was supported by the U.S. Department of Energy, Office of Science, Office of Basic Energy Sciences, under Contract W-31-109-ENG-38.

■ ABBREVIATIONS

WT, wild-type; Ac-DEVD-AFC, acetyl-Asp-Glu-Val-Asp-7-amino-4-trifluoromethylcoumarin; Ac-DEVD-CMK, acetyl-Asp-Glu-Val-Asp-chloromethyl ketone; MD, molecular dynamics; H-bond, hydrogen bond; protomer, large and small subunit obtained by processing a monomer of procaspase-3; PDB, Protein Data Bank.

■ REFERENCES

(1) Boatright, K. M., and Salvesen, G. S. (2003) Mechanisms of caspase activation. *Curr. Opin. Cell Biol. 15*, 725−731.

(2) MacKenzie, S. H., and Clark, A. C. (2012) Death by caspase dimerization. *Adv. Exp. Med. Biol. 747*, 55−73.

(3) Muzio, M., Stockwell, B. R., Stennicke, H. R., Salvesen, G. S., and Dixit, V. M. (1998) An induced proximity model for caspase-8 activation. *J. Biol. Chem. 273*, 2926−2930.

(4) Bose, K., and Clark, A. C. (2001) Dimeric procaspase-3 unfolds via a four-state equilibrium process. *Biochemistry 40*, 14236−14242.

(5) Oberst, A., Pop, C., Tremblay, A. G., Blais, V., Denault, J.-B., Salvesen, G. S., and Green, D. R. (2010) Inducible dimerization and inducible cleavage reveal a requirement for both processes in caspase-8 activation. *J. Biol. Chem. 285*, 16632−16642.

(6) Hardy, J. A., Lam, J., Nguyen, J. T., O'Brien, T., and Wells, J. A. (2004) Discovery of an allosteric site in the caspases. *Proc. Natl. Acad. Sci. U.S.A. 101*, 12461−12466.

(7) Yi, C. H., and Yuan, J. (2009) The Jekyll and Hyde functions of caspases. *Dev. Cell 16*, 21−34.

(8) Sordet, O., Rebe, C., Plenchette, S., Zermati, Y., Hermine, O., Vainchenker, W., Garrido, C., Solary, E., and Dubrez-Daloz, L. (2002) Specific involvement of caspases in differentiation of monocytes into macrophages. *Blood 100*, 4446−4453.

(9) D'Amelio, M., Cavallucci, V., Middei, S., Marchetti, C., Pacioni, S., Ferri, A., Diamantini, A., De Zio, D., Carrara, P., Battistini, L., Moreno, S., Bacci, A., Ammassari-Tuele, M., Marie, H., and Cecconi, F. (2011) Caspase-3 triggers early synaptic dysfunction in a mouse model of Alzermer's disease. *Nat. Neurosci. 14*, 69−76.

(10) Graham, R. K., Ehrnhoefer, D. E., and Hayden, M. R. (2011) Caspase-6 and neurodegeneration. *Trends Neurosci. 34*, 646−656.

(11) Olsson, M., and Zhivotovsky, B. (2011) Caspases and cancer. *Cell Death Differ. 18*, 1441−1449.
(12) McIlwain, D. R., Berger, T., and Mak, T. W. (2013) Caspase functions in cell death and disease. *Cold Spring Harbor Perspect. Biol. 5*, 1−28.
(13) Datta, D., Scheer, J. M., Romanowski, M. J., and Wells, J. A. (2008) An allosteric circuit in caspase-1. *J. Mol. Biol. 381*, 1157−1167.
(14) MacKenzie, S. H., and Clark, A. C. (2013) Slow folding and assembly of a procaspase-3 interface variant. *Biochemistry 52*, 3415−3427.
(15) Pop, C., Feeney, B., Tripathy, A., and Clark, A. C. (2003) Mutations in the procaspase-3 dimer interface affect the activity of the zymogen. *Biochemistry 42*, 12311−12320.
(16) Walters, J., Schipper, J. L., Swartz, P., Mattos, C., and Clark, A. C. (2012) Allosteric modulation of caspase-3 through mutagenesis. *Biosci. Rep. 32*, 401−411.
(17) Feeney, B., Pop, C., Swartz, P., Mattos, C., and Clark, A. C. (2006) Role of loop bundle hydrogen bonds in the maturation and activity of (pro)caspase-3. *Biochemistry 45*, 13249−13263.
(18) MacKenzie, S. H., Schipper, J. L., England, E. J., Thomas, M. E., III, Blackburn, K., Swartz, P., and Clark, A. C. (2013) Lengthening the intersubunit linker of procaspase 3 leads to constitutive activation. *Biochemistry 52*, 6219−6321.
(19) Walters, J., Pop, C., Scott, F. L., Drag, M., Swartz, P., Mattos, C., Salvesen, G. S., and Clark, A. C. (2009) A consitutively active and uninhibitable caspase-3 zymogen efficiently induces apoptosis. *Biochem. J. 424*, 335−345.
(20) Pop, C., Chen, Y.-R., Smith, B., Bose, K., Bobay, B., Tripathy, A., Franzen, S., and Clark, A. C. (2001) Removal of the pro-domain does not affect the conformation of the procaspase-3 dimer. *Biochemistry 40*, 14224−14235.
(21) Walters, J., Swartz, P., Mattos, C., and Clark, A. C. (2011) Thermodynamic, enzymatic and structural effects of removing a salt bridge at the base of loop 4 in (pro)caspase-3. *Arch. Biochem. Biophys. 508*, 31−38.
(22) Bose, K., Pop, C., Feeney, B., and Clark, A. C. (2003) An uncleavable procaspase-3 mutant has a lower catalytic efficiency but an active site similar to that of mature caspase-3. *Biochemistry 42*, 12298−12310.
(23) Davis, I. W., Murray, L. W., Richardson, J. S., and Richardson, D. C. (2004) MolProbity: Structure validation and all-atom contact analysis for nucleic acids and their complexes. *Nucleic Acids Res. 32*, W615−W619.
(24) Feeney, B., Pop, C., Tripathy, A., and Clark, A. C. (2004) Ionic interactions near loop L4 are important for maintaining the active site environment and the dimer stability of (pro)caspase-3. *Biochem. J. 384*, 515−525.
(25) Hess, B., Kutzner, C., van, d. S. D., and Lindahl, E. (2008) GROMACS 4: Algorithms for Highly Efficient, Load-Balanced, and Scalable Molecular Simulation. *J. Chem. Theory Comput. 4*, 435−447.
(26) Wang, J., Cieplak, P., and Kollman, P. A. (2000) How well does a restrained electrostatic potential (RESP) model perform in calculating conformational energies of organic and biological molecules? *J. Comput. Chem. 21*, 1049−1074.
(27) Jorgensen, W. L., Chandrasekhar, J., Madura, J. D., Impey, R. W., and Klein, M. L. (1983) Comparison of simple potential functions for simulating liquid water. *J. Chem. Phys. 79*, 926−935.
(28) Fu, G., Chumanevich, A. A., Agniswamy, J., Fang, B., Harrison, R. W., and Weber, I. T. (2008) Structural basis for executioner caspase recognition of P5 position in substrates. *Apoptosis 13*, 1291−1302.
(29) Wilson, K. P., Black, J.-A. F., Thomson, J. A., Kim, E. E., Griffith, J. P., Navia, M. A., Murcko, M. A., Chambers, S. P., Aldape, R. A., Raybuck, S. A., and Livingston, D. J. (1994) Structure and mechanism of interleukin-1b converting enzyme. *Nature 370*, 270−275.
(30) Keller, N., Mares, J., Zerbe, O., and Grutter, M. G. (2009) Structural and biochemical studies on procaspase-8: New insights on initiator caspase activation. *Structure 17*, 438−448.
(31) Bobay, B. G., Stewart, A. L., Tucker, A. T., Thompson, R. J., Varney, K. M., and Cavanagh, J. (2012) Structural insights into the calcium-dependent interaction between calbindin-D28K and caspase-3. *FEBS Lett. 586*, 3582−3589.
(32) Thomsen, N. D., Koerber, J. T., and Wells, J. A. (2013) Structural snapshots reveal distinct mechanisms of procaspase-3 and -7 activation. *Proc. Natl. Acad. Sci. U.S.A. 110*, 8477−8492.
(33) Velazquez-Delgado, E. M., and Hardy, J. A. (2012) Zinc-mediated allosteric inhibition of caspase-6. *J. Biol. Chem. 287*, 36000−36011.
(34) Alvarado-Kristensson, M., Melander, F., Leandersson, K., Rönnstrand, L., Wernstedt, C., and Andersson, T. (2004) p38-MAPK signals survival by phosphorylation of caspase-8 and caspase-3 in human neutrophils. *J. Exp. Med. 199*, 449−458.
(35) Parrish, A. B., Freel, C. D., and Kornbluth, S. (2013) Cellular mechanisms controlling caspase activation and function. *Cold Spring Harbor Perspect. Biol. 5*, 1−24.
(36) Cao, Q., Wang, X.-J., Liu, C.-W., Liu, D.-F., Li, L.-F., Gao, Y.-Q., and Su, X.-D. (2012) Inhibitory mechanism of caspase-6 phosphorylation revealed by crystal structures, molecular dynamics simulations, and biochemical assays. *J. Biol. Chem. 287*, 15371−15379.
(37) Velazquez-Delgado, E. M., and Hardy, J. A. (2012) Phosphorylation regulates assembly of the caspase-6 substrate-binding groove. *Structure 20*, 742−751.
(38) Callus, B. A., and Vaux, D. L. (2007) Caspase inhibitors: Viral, cellular and chemical. *Cell Death Differ. 14*, 73−78.
(39) Ekici, O. D., Li, Z. Z., Campbell, A. J., James, K. E., Asgian, J. L., Mikolajczyk, J., Salvesen, G. S., Ganesan, R., Jelakovic, S., Grutter, M. G., and Powers, J. C. (2006) Design, synthesis, and evaluation of aza-peptide Michael acceptors as selective and potent inhibitors of caspases-2, -3, -6, -7, -8, -9, and -10. *J. Med. Chem. 49*, 5728−5749.